Journal of Hazardous Materials 416 (2021) 126153

Contents lists available at ScienceDirect

Journal of Hazardous Materials

journal homepage: www.elsevier.com/locate/jhazmat

Research Paper

Uranium re-adsorption on uranium mill tailings and environmental implications

Meiling Yin [a,b,1], Jing Sun [c,1], Hongping He [d], Juan Liu [a], Qiaohui Zhong [a], Qingyi Zeng [e], Xianfeng Huang [f], Jin Wang [a,g,*], Yingjuan Wu [a], Diyun Chen [a,g]

[a] Key Laboratory of Water Quality and Conservation in the Pearl River Delta, Ministry of Education, School of Environmental Science and Engineering, Guangzhou University, Guangzhou 510006, China
[b] School of Environment and Energy, South China University of Technology, Guangzhou 510006, China
[c] State Key Laboratory of Environmental Geochemistry, Institute of Geochemistry, Chinese Academy of Sciences, Guiyang 550081, China
[d] Guangdong Provincial Key Laboratory of Mineral Physics and Materials, Guangzhou Institute of Geochemistry, Chinese Academy of Sciences, Guangzhou 510640, China
[e] School of Resource Environment and Safety Engineering, University of South China, Hengyang 421001, China
[f] School of Life and Environmental Science, Wenzhou University, Wenzhou 325035, China
[g] Guangdong Provincial Key Laboratory of Radionuclides Pollution Control and Resources, Guangzhou 510006, China

ARTICLE INFO

Editor: Dr. Navid B Saleh

Keywords:
Uranium
Solid wastes
Waste management
Re-adsorption mechanism
Remediation indication

ABSTRACT

Uranium mill tailings (UMTs) are one critical source of environmental U pollution. Leaching test has been extensively used to reveal U release capacity and mechanism from UMTs, while little attention has been paid to the effects of re-adsorption process on U release. In this study, the role of U re-adsorption behaviors during leaching test with UMTs was comprehensively investigated. Through paired data on mineralogical composition and aqueous U speciation, the influence of environmentally relevant factors on U re-absorption capacity and mechanism on UMTs with different particle sizes was revealed. Significant amounts of U re-adsorption were observed and primarily attributed to the adsorption on chlorite, albite and muscovite as well as combined reduction-sequestration by muscovite. Uranium re-adsorption predominantly occurred via inner-sphere complexation and surface precipitation depending on leachant pH. Coexisting sulfate or phosphate could further enhance U re-adsorption. The enhanced re-adsorption from sulfate occurred when inner-sphere complexation governed the re-adsorption process. These findings suggest that the environmental hazards and ecological risks of the U containing (waste) solids might have been underestimated due to the ignorance of the re-adsorption process, since the re-adsorbed U could be easily re-mobilized. The insights from this study are also helpful in developing effective in-situ remediation strategies.

1. Introduction

Uranium (U) is a naturally occurring radioactive material, which has high toxicity and radioactivity (Kong et al., 2018; Kuhar et al., 2018; Sun et al., 2019; Wang et al., 2020; Yin et al., 2021). Uranium-contaminated soil and aquifer systems resulting from the legacy of extraction and processing of U ore and radioactive waste disposal are a long-term environmental problem worldwide (Petrescu and Bilal, 2003; Winde, 2013; Chang and Zhou, 2017; Yang et al., 2019), posing serious hazards to human health and ecosystem stability (Antunes et al., 2008; Sharma, 2012; Pan et al., 2021). To date, despite intensive research, the processes resulting in longevity of high levels of solution and solid U at contaminated sites are still not fully understood. As a result, even after extensive clean-up efforts, dissolved U concentrations at contaminated sites often remain above regulatory limits (Chevychelov and Sobakin, 2017; Wang et al., 2017; Godoy et al., 2019).

Uranium mill tailings (UMTs) are a major U contamination source (Abdelouas, 2006; Ballini et al., 2020; Wang et al., 2021). To mitigate UMT-induced U contamination, it is necessary to understand the behavior and fundamental mechanism of U release from UMTs under

* Corresponding author at: Key Laboratory of Water Quality and Conservation in the Pearl River Delta, Ministry of Education, School of Environmental Science and Engineering, Guangzhou University, Guangzhou 510006, China.
E-mail address: wangjin@gzhu.edu.cn (J. Wang).
[1] These authors contributed equally to this work.

https://doi.org/10.1016/j.jhazmat.2021.126153
Received 16 January 2021; Received in revised form 15 May 2021; Accepted 15 May 2021
Available online 18 May 2021

environmentally relevant conditions. Leaching test can be an effective tool to investigate U release behavior under varied conditions. Using leaching tests, the effects of a variety of geochemical factors, including pH, temperature, particle size, natural organic matter and mineralogical constituent on U release have been investigated (Liu et al., 2017; Kanzari et al., 2017; Yin et al., 2019; Li et al., 2019a; Ge et al., 2020). Based on the findings, U adsorption on natural minerals presented in the UMTs was recognized to be a vital process affecting U solubility and migration (Lee et al., 2011). Relevant studies also suggested that re-adsorption during leaching is of crucial importance for the release of U and many other metals including Cu and Pb from soil (Zhang et al., 1998; Peng et al., 2018), and ore materials (Hamza, 2018; Nada et al., 2019). Re-adsorption process, therefore, can affect the longevity of heavy metals at contaminated sites and the risk of human exposure. However, the critical factors and mechanism influencing U re-adsorption process on post-leaching UMTs are largely unstudied.

The objectives of this study were thus to (i) explore the effects of environmentally relevant factors encountered at UMTs on U re-adsorption behavior and (ii) investigate the interfacial mechanism of U re-adsorption on UMTs. Batch re-adsorption kinetic experiments as well as adsorption isotherms and pH envelopes were conducted. Aqueous U speciation and mineralogical transformation in these batch re-adsorption experiments were investigated by several analytical techniques as well as solution U speciation modeling. The insights into U re-adsorption processes can improve our understanding of the rationale of re-adsorption based U (im)mobilization process and also aid in developing effective remediation strategy for UMTs/other (waste) solids contamination.

2. Materials and methods

2.1. Site information

The Xiazhuang U ore field located in Shaoguan, Guangdong Province, China, is a crucial contributor of U resource in China. This ore field contains 18 U deposits with total U resource estimated to be 12,000 t (Wang et al., 2019). Uranium in the ore deposits is predominantly associated with colloidal pyrite, pink microcrystalline quartz, hydrogoethite, and hematite (Liu et al., 2018). More than 50 years of exploitation and hydrometallurgy have resulted in serious contamination of U and other co-occurring heavy metals (e.g., Th, Cu, Pb and Mn) in the surrounding environment, posing detrimental effects on local ecosystem (Wang et al., 2012; Liu et al., 2015; Chen et al., 2017). The UMT samples were assembled from the tailings dam, which serves as a waste container of a large U hydrometallurgy plant. More information on the study site and UMT sample collection could be referred elsewhere (Yin et al., 2019).

2.2. Sample selection and pre-treatment

After being air-dried, the UMTs samples were separated into different particle size fractions, i.e., 6–10, 2–6, 0.9–2, 0.45–0.9, and less than 0.45 mm using nylon screen with different diameters. Their weight proportions are 34.3%, 25.3%, 10.8%, 9.2% and 20.5%, respectively. UTMs with particle diameters of 6–10 mm ($UMT_{6–10\ mm}$) and less than 0.45 mm ($UMT_{<0.45\ mm}$) were selected to perform U re-adsorption experiments in this study. The reasons for choosing these two size fractions were that (i) $UMT_{6–10\ mm}$ and $UMT_{<0.45\ mm}$ are the two most dominant fractions in UMTs and represent the maximum and minimum grain sizes, respectively; (ii) considerable quantities of carbonate extractable U(VI) (the U fraction that can be extracted by Na_2CO_3/$NaHCO_3$) was observed in both $UMT_{6–10\ mm}$ and $UMT_{<0.45\ mm}$, which can be mobilized and re-adsorbed during leaching; and (iii) the bulk mineral compositions of $UMT_{6–10\ mm}$ and $UMT_{<0.45\ mm}$ are significantly different, which may leads to different U re-adsorption capacities and mechanisms (Giammar and Hering, 2001; Rout et al., 2015).

To prepare post-leaching UMTs and avoid the affect of indigenous U in UMTs, prior to re-adsorption experiments, $UMT_{6–10\ mm}$ and $UMT_{<0.45\ mm}$ were pre-treated with a mixed carbonate solution with 14.4 mM $NaHCO_3$ and 2.8 mM Na_2CO_3 to remove labile U(VI), following the procedures of Liu et al. (2013). $UMT_{6–10\ mm}$ and $UMT_{<0.45\ mm}$ were further washed with U-free solutions identical with those used in the re-adsorption test until U concentration in the leachate was below 4.2×10^{-8} M, which was one order of magnitude lower than the minimum initial U concentration used in re-adsorption test.

2.3. Batch Re-adsorption experiments

To ascertain how U(VI) re-adsorption on post-leaching UMT proceeds over time, kinetic experiments were conducted. In each kinetic experiment, 0.2 g of air-dried post-leaching UMT sample was dispersed in 20 mL of ambient 0.01 M NaCl in a 50 mL polyethylene tube. The solid-to-liquid ratio of 10 g L^{-1} was consistent with the ratio in ANS 16.1 leaching test (ANS, 1986). The pH value of the resulting suspension was buffered with 0.05 M potassium hydrogen phthalate, monitored by a calibrated pH electrode and adjusted to the desired pH value of 4.0 with 0.1 M H_2SO_4. H_2SO_4 was selected to adjust the pH value to 4.0, because the sample site is commonly subjected to sulfuric acid rain and the common pH value of acid rain in the studied area is around 4.0. Then 6.3×10^{-5} M U(VI) was added to the suspension from a freshly prepared U(VI) stock solution. The U(VI) stock solution (6.3×10^{-3} M) was obtained by dissolving $UO_2(NO_3)_2•6H_2O$ in Milli-Q H_2O. Aliquots (i.e., UTM-solution mixture) were removed from the suspension at various time intervals over 120 h and filtered using 0.45-μm nylon membrane filters. The solution subsamples were acidified to 2% HNO_3 and analyzed by inductively coupled plasma mass spectrometry (ICP-MS).

The extent of U re-adsorption on post-leaching UMTs can change with U concentration and pH (Hongxia and Zuyi, 2002; Jin et al., 2016). Thermodynamic re-adsorption experiments as a function of U concentration at constant pH (isotherms) and as a function of pH at constant U concentration (pH envelopes) were therefore conducted. To perform isotherm experiments, air-dried post-leaching UMT samples were dispersed in 0.01 M NaCl solutions in 50 mL polypropylene tubes. The pH value of the resulting suspensions was buffered with 0.05 M potassium hydrogen phthalate and adjusted to pH 4.0. Uranium(VI) was then added with initial U concentrations of 4.2×10^{-7} to 6.3×10^{-4} M from the stock solution. The pH envelopes were conducted on a series of buffered U(VI) solutions, in which the added U concentration was 6.3×10^{-5} M. The suspensions used in the pH envelopes were created by dispersing air-dried post-leaching UMT samples in 0.01 M NaCl solutions and varying pH between 2.0 and 8.0. The pH was maintained with 0.05 M potassium hydrogen phthalate-H_2SO_4 (NaOH) and 0.01 M sodium borate decahydrate-H_2SO_4. To investigate the effect of ionic strength on U re-adsorption, parallel pH envelopes were performed by dispersing post-leaching UMT samples in 0.1 M NaCl. Various ligands can form soluble uranyl complexes and/or insoluble minerals with U (VI), which affects the U re-adsorption behavior (Fan et al., 2014). To reveal the influence of ligand (sulfate and phosphate) type, additional pH envelopes between 2.0 and 8.0 were conducted by dispersing post-leaching UMT samples in 0.01 M sulfate or 0.01 M phosphate solutions. Sulfate was chosen because sulfuric acid is the leaching agent for UMTs (Yin et al., 2019). Phosphate was used because the formation of meta-autunite ($Ca(UO_2)_2(PO_4)_2•3H_2O$) was previously detected in post-leaching UMT (Yin et al., 2019). Sulfate and phosphate in these pH envelopes were added as Na_2SO_4 and Na_2HPO_4, respectively. All of the kinetic and isothermal re-adsorption experiments were performed in triplicate, and chemicals used in the experiments were obtained from the Chemical Reagent Factory (Guangzhou, China).

2.4. Analytical procedures

2.4.1. Solution-phase characterization

Dissolved U concentrations in the samples from the batch re-adsorption experiments were determined by ICP-MS (Thermal X series 2) using previously published procedures (Li et al., 2019b). Rhodium (Rh) was selected as an internal response standard and used to monitor potential instrument drift. To accurately calculate the added concentrations of internal response standard and the dilution factors of the samples, the ICP-MS samples were prepared by weighing method. A 4-point standard curve obtained by a multi-element standard was used to quantify U concentration. The analytical accuracy of within 3% was observed against known reference materials W-2a (Centerville Diabase-212) and BHVO-2 (Hawaiian Basalt-1207).

2.4.2. Solid-phase characterization

Bulk mineralogy in $UMT_{6–10\ mm}$ and $UMT_{<0.45\ mm}$ was determined by X-ray diffraction (XRD) and the detailed analytical and data reduction methods can be referred to Yin et al. (2019). To assess the distribution of the re-adsorbed U on post-leaching UMTs, post-re-adsorption UMTs were analyzed by back scattered electron imaging as well as energy dispersive spectrometer (BSE-EDS). The BSE-EDS analysis was executed with a field emission scanning electron microscope (FESEM, SU8010, Hitachi, Japan). To reveal solid-phase U speciation, post-re-adsorption UMTs were determined by X-ray photoelectron spectroscopy (XPS, Thermo Fisher K-alpha). XPS spectra were processed in Thermo Scientific Avantage software following the procedures of Ilton et al. (2005). The binding energy (BE) of C 1s line for aliphatic carbon (284.8 eV) was used to correct charge. A spin-orbit splitting of 10.89 eV was adopted to fit the doublet peaks of U 4f spectra. Uranium speciation was calculated based on the U 4f/5 peaks because U 4f/7 peaks were subject to the effect of K 2 s

2.5. Thermodynamic solution speciation modeling

Solution U speciation can be an important factor decisive to U re-adsorption behavior (Fan et al., 2014; Jin et al., 2016). The equilibrium solution U speciation in the batch re-adsorption experiments were calculated by the geochemical code PHREEQC-2. The reactions and equilibrium constants used for the calculation (Table S1) were mainly from the standard PHREEQC database llnl.dat, which was further updated with the most recent U thermodynamic data from OECD/NEA (Guillaumont and Mompean, 2003). Input parameters include pH, Eh, temperature, partial pressure of CO_2, dissolved U concentration, and the type and concentration of the ligand (i.e., chloride, sulfate and phosphate).

3. Results and discussion

3.1. Re-adsorption kinetics

As observed in the conducted kinetic experiments, U re-adsorption on post-leaching UMTs at pH 4.0 was rapid, and the equilibrium could be achieved within 24 h (Fig. 1a). Similar rapid U adsorption was also observed on, for example, silica (Guo et al., 2009), muscovite (Arnold et al., 2006), illite (Liao et al., 2020) and chlorite (Singer et al., 2009), all of which are dominant minerals in the studied UMTs (Yin et al., 2020). Pseudo-first order (Eq. (1)) and pseudo-second order (Eq. (2)) equations were used to describe the kinetics of U re-adsorption on post-leaching UMTs (Ho and Mckay, 1999):

$$\ln[q_e - q(t)] = \ln \quad q_e - k_1 t \tag{1}$$

$$\frac{t}{q(t)} = \frac{t}{q_e} + \frac{1}{k_2 q_e^2} \tag{2}$$

where k_1 (h^{-1}) and k_2 (g mol^{-1} h^{-1}) represent the pseudo-first order and pseudo-second order rate constants, respectively, q_t (mol g^{-1}) is the amount of re-adsorbed U at time t (h), and q_e (mol g^{-1}) is the amount at equilibrium. Based on the coefficient of determination (R^2), the description of kinetic data using the pseudo-second order equation ($UMT_{6–10\ mm}$: $R^2 = 0.996$; $UMT_{<0.45\ mm}$: $R^2 = 0.999$) (Fig. 1b) is preferable as compared to the pseudo-first order equation ($UMT_{6–10\ mm}$: $R^2 = 0.997$; $UMT_{<0.45\ mm}$: $R^2 = 0.851$) (Fig. S1), as is the case for U adsorption on granite (Jin et al., 2016). The pseudo-second order rate constants (k_2) of U(VI) re-adsorption on $UMT_{6–10\ mm}$ and $UMT_{<0.45\ mm}$ were both around 250 g mol^{-1} h^{-1}. The amounts of re-adsorbed U (q_e) on $UMT_{6–10\ mm}$ and $UMT_{<0.45\ mm}$ at equilibrium were 3.0 and 5.3 μmol g^{-1}, respectively.

3.2. Effects of different environmentally relevant factors

3.2.1. Added uranium concentration

The influence of varied U concentration on U re-adsorption during leaching test was investigated through isotherm experiments. For both post-leaching $UMT_{6–10\ mm}$ and $UMT_{<0.45\ mm}$, the U re-adsorption isotherms at pH 4.0 showed substantial re-adsorption at low added U(VI) concentrations and a clear asymptote in the amounts of adsorbed U (Fig. 2a). Therefore, two-parameter and three-parameter isotherm models were chosen to describe the U re-adsorption isotherms in this study. Our isotherm data were more effectively fitted with the *Langmuir* equation (Eq. (3)) (Langmuir, 1918) (Fig. 2b) as compared with other two-parameter isotherm models (*Freundlich and Temkin*) (Fig. S2). Three-parameter isotherm model, *Sips* isotherm (Eq. (4)) (Sips, 1948)

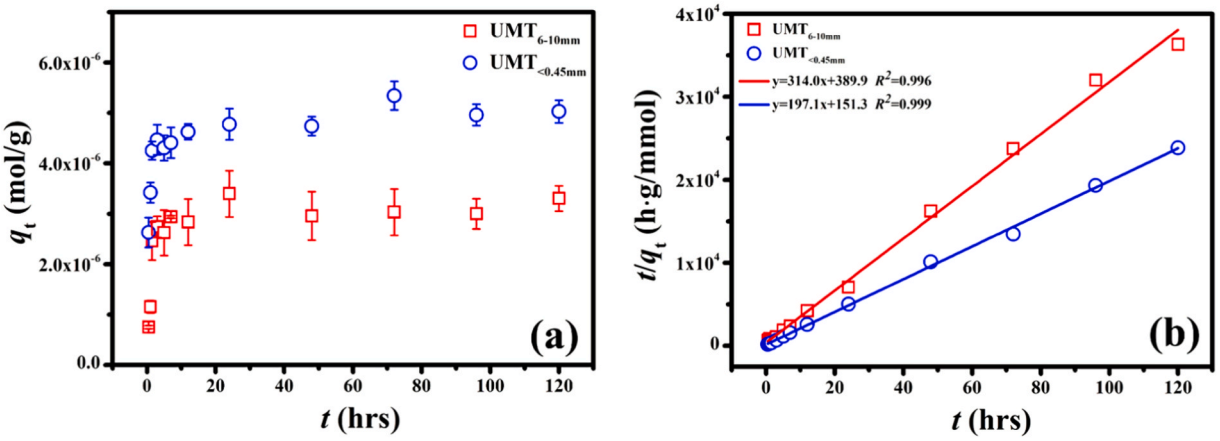

Fig. 1. Re-adsorption kinetics (a) and pseudo-second order rate equation fitting (b) of U (VI) on $UMT_{6–10\ mm}$ and $UMT_{<0.45\ mm}$ under the conditions of $C_0 = 6.3 \times 10^{-5}$ mol L^{-1}, pH = 4.0, $m/V = 10$ g L^{-1}, $T = 25$ °C, $I = 0.01$ mol L^{-1} NaCl.

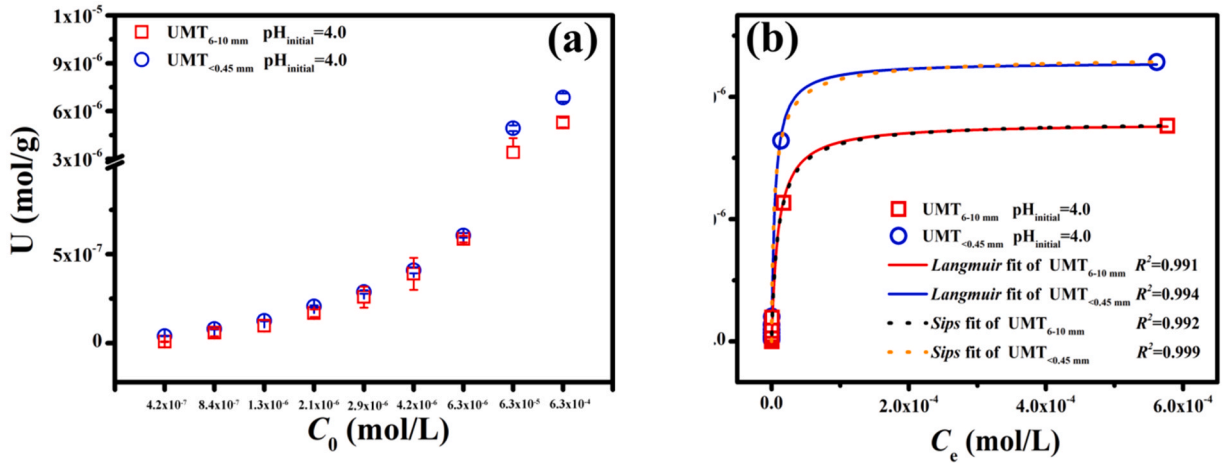

Fig. 2. Effects of U initial concentration on U re-adsorption to $UMT_{6–10\ mm}$ and $UMT_{<0.45\ mm}$ (a) and *Langmuir* model and *Sips* isotherm fitting (b) under the conditions of $m/V = 10$ g L^{-1}, pH = 4.0, $T = 25$ °C, $I = 0.01$ mol L^{-1} NaCl.

(Fig. 2b) can also be well scrutinized for equilibrium data. According to the results of *Langmuir* and *Sips* isotherm fitting, the maximum adsorption capacities (q_m) of post-leaching $UMT_{<0.45\ mm}$ and $UMT_{6–10\ mm}$ for U (VI) were estimated to be 6.9 (*Langmuir*) / 7.0 (*Sips*) and 5.4 μmol g^{-1}, respectively (Table S2), both were significantly higher than that of the un-treated granite (2.4 μmol g^{-1}) (Jin et al., 2016). The exponent 1/n value of $UMT_{6–10\ mm}$ (0.926) was more closer to unity than that of $UMT_{<0.45\ mm}$ (0.780), indicating that U re-adsorption on $UMT_{6–10\ mm}$ best fits *Langmuir* form and inclines to mono-layer adsorption (Guenay et al., 2007). Moreover, Gibbs energy change ($\triangle G$) at ambient temperature (298.15 K) is used to evaluate the feasibility of adsorption. According to the results of *Langmuir* isotherm fitting (Table S2), the *b* values of $UMT_{6–10\ mm}$ and $UMT_{<0.45\ mm}$ were 104.4 and 202.2 L $mmol^{-1}$, respectively. Based on Eqs. (5) and (6) (Hai et al., 2017), $\triangle G$ values were calculated to be − 38.6 and − 40.2 kJ mol^{-1} for $UMT_{6–10\ mm}$ and $UMT_{<0.45\ mm}$, respectively. Therefore, U re-adsorption on $UMT_{6–10\ mm}$ and $UMT_{<0.45\ mm}$ is both favorable.

Langmuir model:

$$q_e = \frac{q_m b C_e}{1 + b C_e} \tag{3}$$

Sips isotherm:

$$q_e = \frac{q_m a_s C_e^{1/n}}{1 + a_s C_e^{1/n}} \tag{4}$$

Where q_e (mol g^{-1}) and C_e (mol L^{-1}) correspond to the amount of adsorbed U and aqueous U concentration at equilibrium, respectively; q_m (mol g^{-1}) represents the maximum adsorption capacity and *b* (L mol^{-1}) denotes the *Langmuir* constant; a_s indicates *Sips* constant associated with adsorption energy; When the exponent $1/n = 1$, *Sips* isotherm reduces to the *Langmuir* equation.

Gibbs energy change (ΔG):

$$\Delta G = -RT\ln(K_C) \tag{5}$$

$$K_C = 55{\cdot}5 \times b \tag{6}$$

Where ΔG is the Gibbs energy change (J mol^{-1}), *R* and *T* indicate the universal gas constant (8.314 J mol^{-1} K^{-1}) and the adsorption temperature (K), respectively, and K_C represents the thermodynamic equilibrium constant, which can be obtained by multiplying *Langmuir* constant *b* (L mol^{-1}) and 55.5 (pure water, mol L^{-1}).

With similar concentrations of added U(VI), re-adsorbed U on $UMT_{<0.45\ mm}$ was constantly higher than that on $UMT_{6–10\ mm}$ (Fig. 2a). The phenomenon of more extensive U re-adsorption on $UMT_{<0.45\ mm}$ as compared to $UMT_{6–10\ mm}$ was also observed in the re-adsorption kinetic experiments (Fig. 1). Based on PHREEQC calculated solution speciation, UO_2^{2+} was always the primary solution species under the experimental conditions used in the isotherm and kinetic experiments (Fig. 3). At pH < 5.0, UO_2^{2+} is usually adsorbed on clay minerals (Korichi and Bensmaili, 2009). Nevertheless, elevated amount of clay minerals was observed in $UMT_{6–10\ mm}$ rather than $UMT_{<0.45\ mm}$ (Fig. S3). Apart from adsorption on clay minerals, there must be another predominant mechanism behind the higher U re-adsorption capacity of $UMT_{<0.45\ mm}$.

3.2.2. pH

The adsorption of U, like many other metal ions (Sun et al., 2016), is pH dependent (Fig. 4). Based on the conducted pH envelopes, the amount of re-adsorbed U on $UMT_{<0.45\ mm}$ was extremely low at pH 2.0 and 3.0, and significantly increased when pH was above 4.0 (Fig. 4b). Based on equilibrium solution U speciation calculated using PHREEQC (Fig. 4c, d), U mainly existed in the form of UO_2^{2+} in pH 2.0 and 3.0, whereas schoepite ($4UO_3{\bullet}9H_2O$) would form at pH > 4.8 and lead to significantly elevated amount of re-adsorbed U on $UMT_{<0.45\ mm}$. The pattern of U re-adsorption on $UMT_{6–10\ mm}$ differed from that on $UMT_{<0.45\ mm}$, with significantly less extensive re-adsorption occurring at pH > 6.0 (Fig. 4a). The distinctive U re-adsorption behaviors between $UMT_{6–10\ mm}$ and $UMT_{<0.45\ mm}$ might originate from their different mineral compositions, which could result in different solution U speciation. For instance, $UMT_{6–10\ mm}$ contained a higher amount of calcite than $UMT_{<0.45\ mm}$ (Fig. S3), (Yin et al., 2020) which can suppress U re-adsorption by forming uranyl carbonate solution complexes including

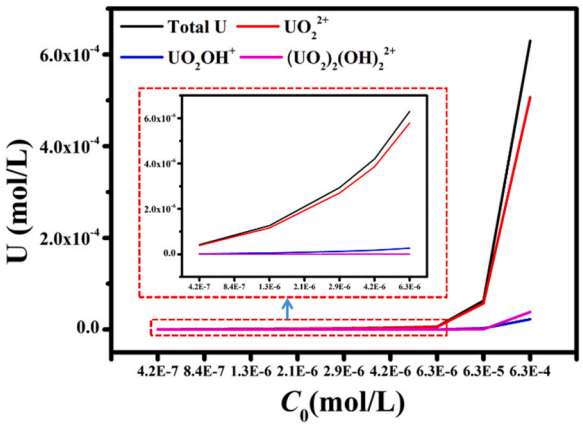

Fig. 3. Aqueous U speciation at different initial U concentrations under the conditions of $m/V = 10$ g L^{-1}, pH = 4.0, $T = 25$ °C, $I = 0.01$ mol L^{-1} NaCl.

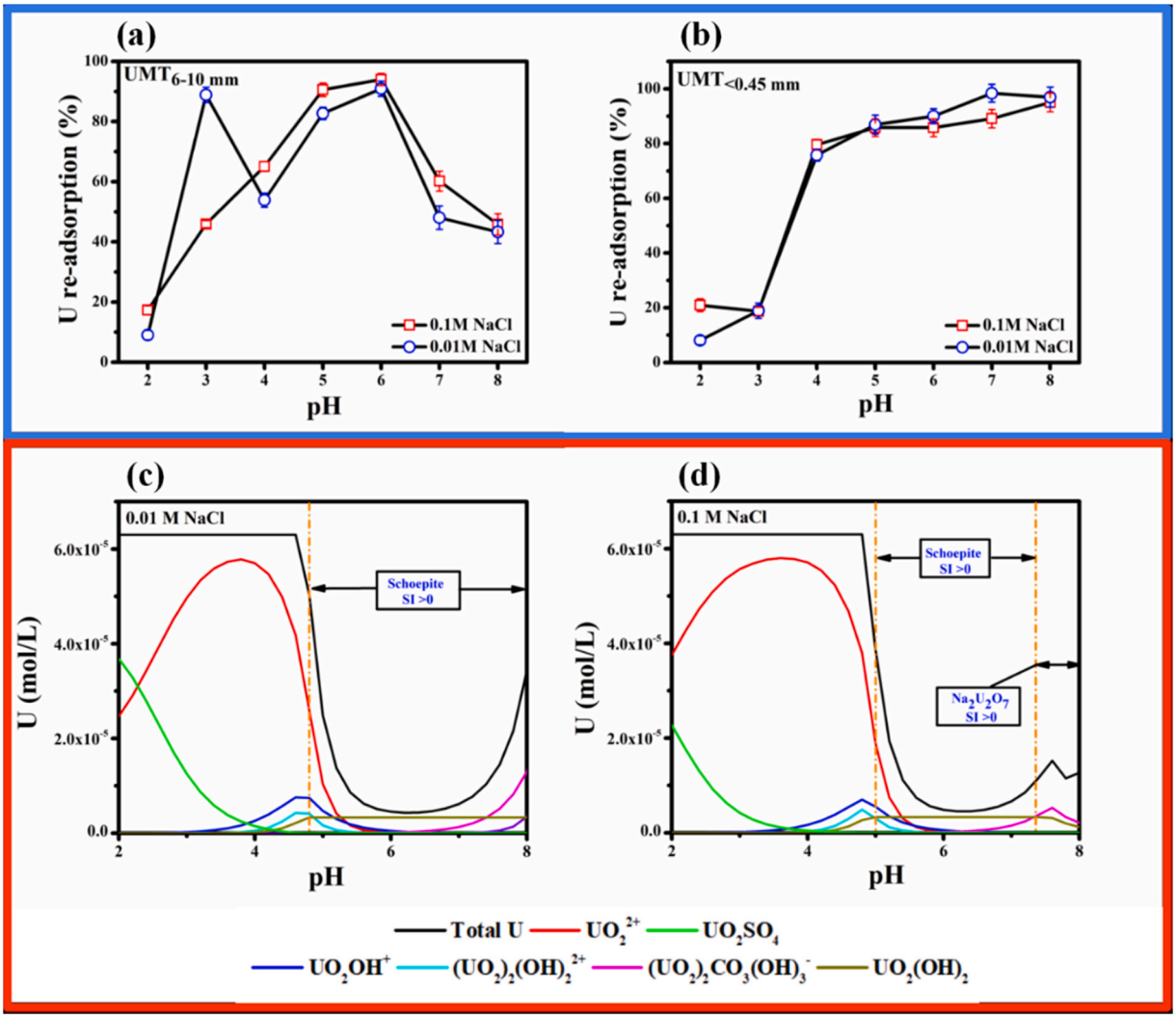

Fig. 4. Effects of pH and ionic strength on U re-adsorption (a, b) and aqueous U speciation (c, d) in $UMT_{6–10\ mm}$ and $UMT_{<0.45\ mm}$ at $C_0 = 6.3 \times 10^{-5}$ mol L^{-1} under the conditions of $m/V = 10$ g L^{-1}, $T = 25$ °C.

$(UO_2(CO_3)_2^{2-}$, $UO_2)_2CO_3(OH)_3^-$ and $UO_2(CO_3)_3^{4-}$ (Kipp et al., 2009; Qiang et al., 2016).

3.2.3. Ionic strength

To unravel the effect of ionic strength on U re-adsorption, pH envelopes were performed with background electrolyte of 0.01 M and 0.1 M NaCl (Fig. 4a, b). Except for $UMT_{6–10\ mm}$ at pH 3.0, the weaker influences of ionic strength on U re-adsorption in $UMT_{6–10\ mm}$ and $UMT_{<0.45\ mm}$ were found as compared with that of pH. Higher ionic strength inhibited U re-adsorption on $UMT_{6–10\ mm}$ at pH 3.0. Previous studies suggested that, U re-adsorption on $UMT_{6–10\ mm}$ and $UMT_{<0.45\ mm}$ under varied pHs was mainly regulated by internal complexation and surface precipitation, while ion exchange and external complexation mainly affected U re-adsorption on $UMT_{6–10\ mm}$ at pH 3.0 (Shao et al., 2009; Fan et al., 2011; Jin et al., 2016). Based on PHREEQC calculation (Fig. 4c, d), solution U speciation was identical when the concentration of the background electrolyte of NaCl was changed from 0.01 M to 0.1 M. Therefore, the influence of ion strength on U re-adsorption was not related to aqueous U speciation. Clay minerals tended to combine with U(VI) by cation exchange or surface complexation, while the former would be more prevailing in acidic environment (Turner et al., 1996). Based on XRD results (Fig. S3), muscovite and chlorite were main clay minerals in $UMT_{6–10\ mm}$. Moreover, the cooperative relationship rather than the competitive effect between cations and UO_2^{2+} was found in U adsorption on muscovite (Lee et al., 2009). Therefore, the elevated U re-adsorption on $UMT_{6–10\ mm}$ at pH 3.0 was probably controlled by cation exchange of chlorite.

3.2.4. Ligand type

The type of ligands can affect the U re-adsorption behavior, because different ligands can promote the formation of different U-bearing solution complexes or minerals (Kang et al., 2002; Gavrilescu et al., 2009). The influences of phosphate and sulfate on U re-adsorption were elucidated in this study (Fig. 5a). Consistent with previous studies (Bostick et al., 2002; Pan et al., 2011), enhanced U re-adsorption was observed in the presence of 0.01 M phosphate as compared to 0.01 M chloride (except in the pH = 2.0 condition). The pH envelopes of U re-adsorption on $UMT_{6–10\ mm}$ and $UMT_{<0.45\ mm}$ were almost identical with more than 90% of the added U re-adsorbed at pH ≥ 3.0. With 0.01 M phosphate, U predominantly existed as soluble $UO_2(H_2PO_4)_2$ at pH < 3.6, while $(UO_2)_3(PO_4)_2{\bullet}4H_2O$ would precipitate at pH > 3.6 and thus led to high fraction of re-adsorbed U (Fig. 5c). Additionally, the formation of ternary complexes on UMTs surface, which bear U and phosphate, may promote U re-adsorption, which had also been observed on ferrihydrites (Payne et al., 1996), goethite-coated sand (Cheng et al., 2004), kaolinite (Liang et al., 2010) and montmorillonite (Troyer et al., 2016). As for 0.01 M sulfate, the amount of re-adsorbed U on $UMT_{<0.45\ mm}$ increased with pH increasing from 3.0 to 8.0, while the amount of re-adsorbed U

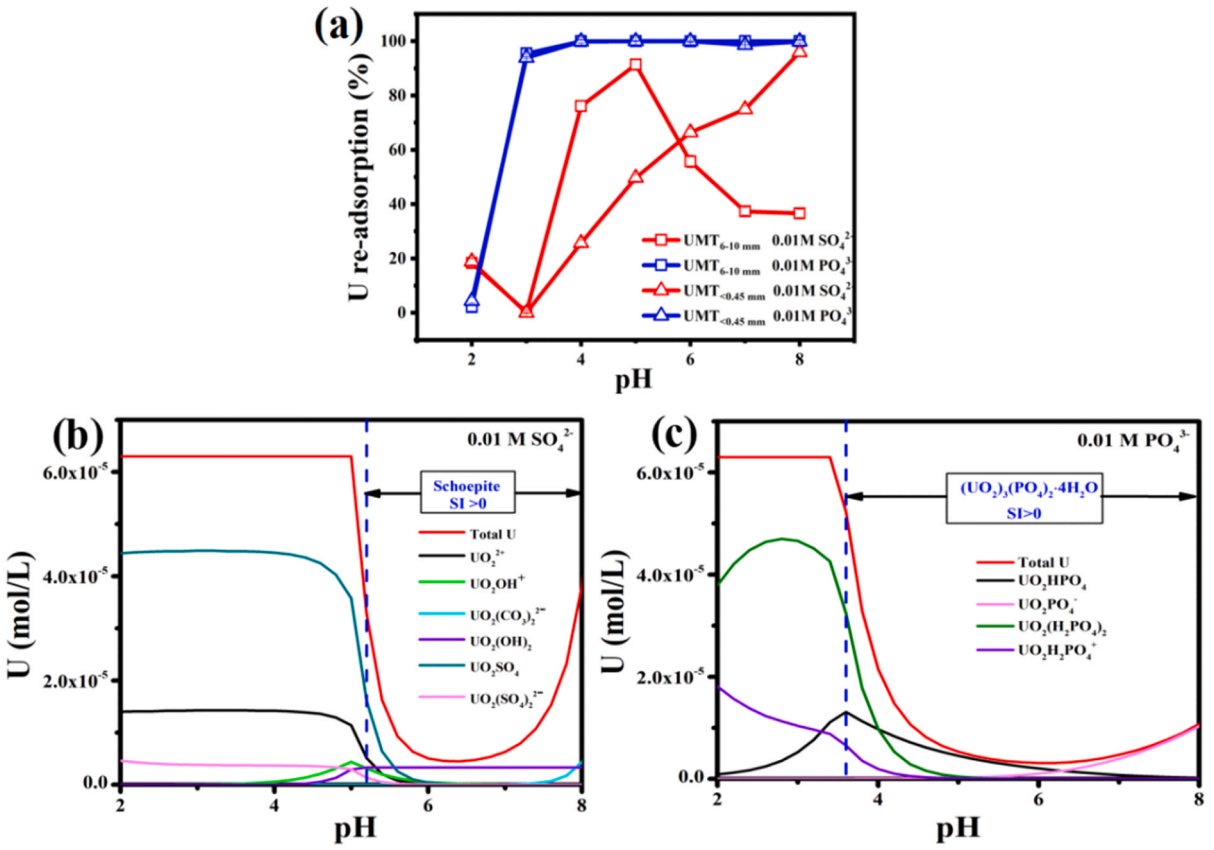

Fig. 5. Variations of U re-adsorption rate (a) and aqueous U speciation (b, c) in $UMT_{6–10\ mm}$ and $UMT_{<0.45\ mm}$ as a function of pH at 0.01 M SO_4^{2-} and 0.01 M PO_4^{3-} under the conditions of $C_0 = 6.3 \times 10^{-5}$ mol L^{-1}, $m/V = 10$ g L^{-1}, $T = 25$ °C.

on $UMT_{6–10\ mm}$ had a broad maximum at pH 5.0. UO_2SO_4 and UO_2^{2+} were the most dominant U species between pH 2.0 and 5.2, while the precipitation of schoepite would occur at pH > 5.2, which might have led to the maximum of U re-adsorption observed at pH 5.0 (Fig. 5b). The decline in U re-adsorption on $UMT_{6–10\ mm}$ with further increased pH can be attributed to the occurrence of highly soluble $UO_2(CO_3)_2^{2-}$ (Barnett

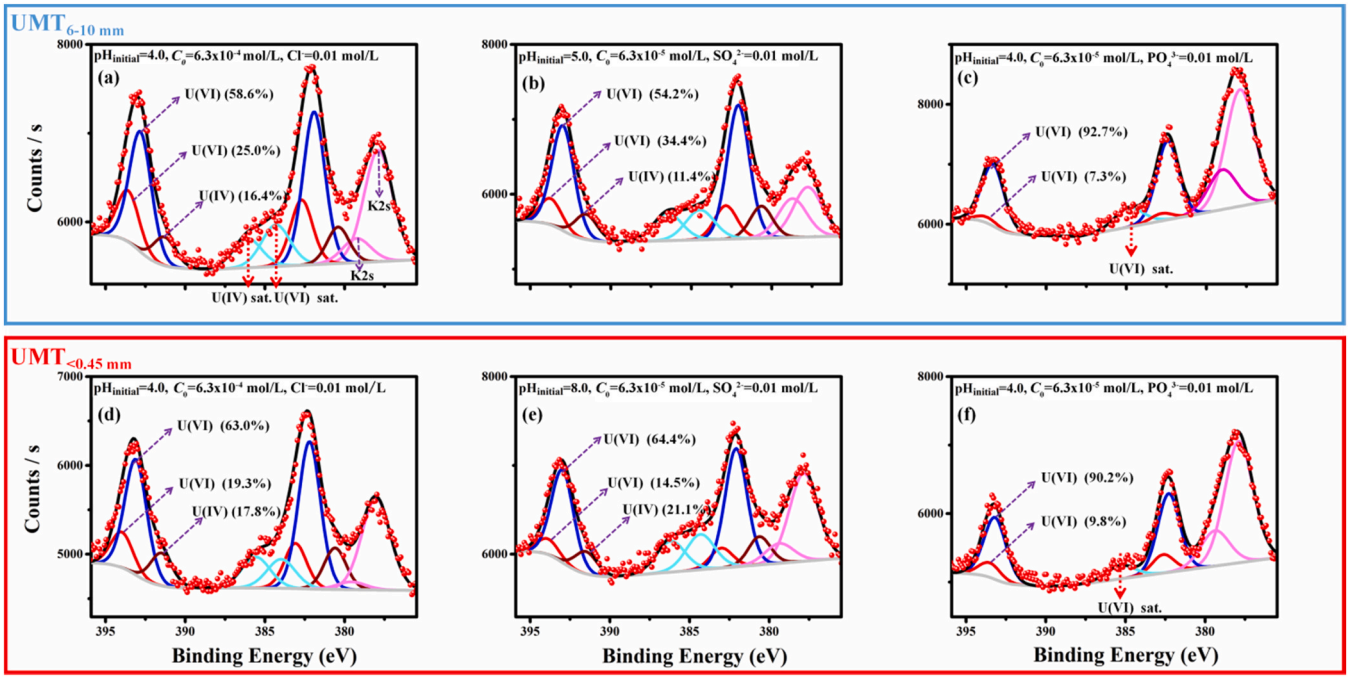

Fig. 6. Fitted U 4f XPS spectra for $UMT_{6–10\ mm}$ (a–c) and $UMT_{<0.45\ mm}$ (d–f) after U re-adsorption under different conditions. Raw data was displayed with discrete points and fitted curves with solid lines.

et al., 2002; Jo et al., 2018), because $UMT_{6–10\ mm}$ contained considerable amount of calcite and thereby was conducive to the formation of uranyl carbonates. In addition, at pH < 5.2, when excluding the effect of schoepite, it was found that 0.01 M sulfate promotes U re-adsorption on $UMT_{6–10\ mm}$ as compared with 0.01 M chloride except for pH = 3.0 (Figs. 5a, 4a). Therefore, elevated U re-adsorption capacity can be obtained with the occurrence of phosphate or sulfate, which leads to the formation of complexes promoting U re-adsorption during leaching test, excluding the condition of pH = 3.0, when U re-adsorption was mainly controlled by cation exchange of clay minerals. Moreover, remarkable U re-adsorption capacity observed in the occurrence of phosphate than sulfate can be attributed the better affinity of phosphate on UMTs surface, which had also been observed in U adsorption on kaolinite (Liang et al., 2010).

3.3. Uranium Re-adsorption mechanism

To identify and quantify solid-phase U speciation, post-re-adsorption UMTs were analyzed by XPS. XPS U(4f) spectra of $UMT_{6–10\ mm}$ (Fig. 6a–c) were slightly shifted to lower BEs as compared to those of $UMT_{<0.45\ mm}$ (Fig. 6d–f). For both post-re-adsorption $UMT_{6–10\ mm}$ (Fig. 6a) and $UMT_{<0.45\ mm}$ (Fig. 6d) from the experiments with 0.01 M chloride, their XPS U(4f) spectra contained a reduced U(IV) faction with the low BEs at ~380.5 eV and corresponding shake-up satellites (Teterin and Teterin, 2004). Uranium(VI) reduction in both $UMT_{6–10\ mm}$ and $UMT_{<0.45\ mm}$ might result from the existence of muscovite (Fig. S4), which contains Fe(II) and has been corroborated to be able to reduce U (VI) even in aerobic environment (Ilton et al., 2006; Arnold et al., 2006). Moreover, the decreased intensities of muscovite d_{001} signals were observed in post-re-adsorption $UMT_{6–10\ mm}$ and $UMT_{<0.45\ mm}$ as compared to pre-re-adsorption UMTs (Fig. S4), indicating that the

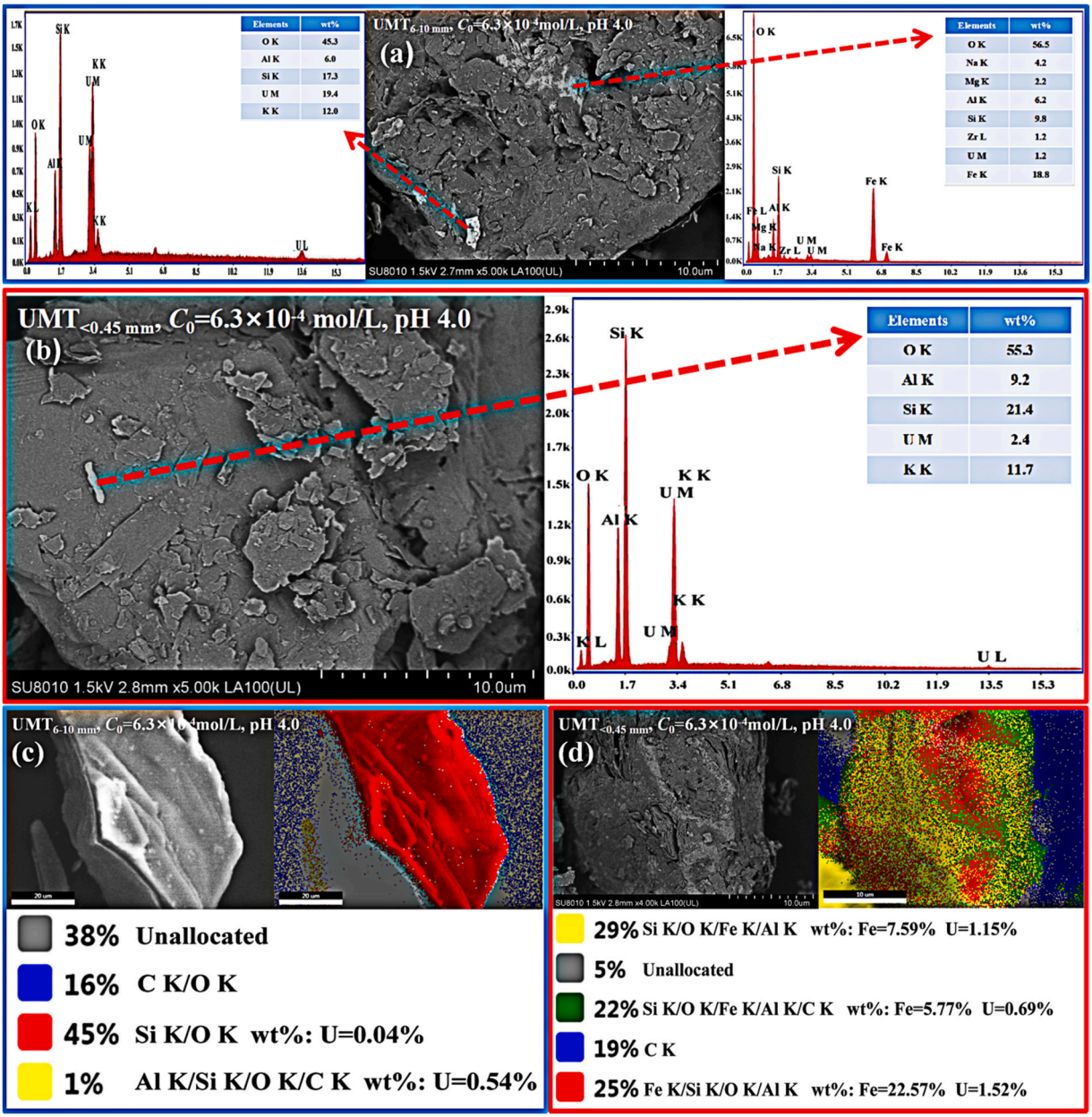

Fig. 7. BSE images and mapping of $UMT_{6–10\ mm}$ (a, c) and $UMT_{<0.45\ mm}$ (b, d) after U re-adsorption at $C_0 = 6.3 \times 10^{-4}$ mol L^{-1}, pH = 4.0. EDS results of brighter area indicated the site where U enrichment was observed. Different phases were distinguished by different colors in BSE mapping images. (For interpretation of the references to colour in this figure legend, the reader is referred to the web version of this article.)

interlayer spacing of muscovite had been altered during U(VI) reduction. Two U(VI) species with separate coordination environments were present in post-re-adsorption $UMT_{6–10\ mm}$ and $UMT_{<0.45\ mm}$ (Fig. 6a, d). BSE-EDS analysis was used for the assignation of these U(VI) species (Fig. 7). Due to its high atomic number, the distribution of U was easily identified in BSE. Meanwhile, the elemental composition of the brighter area where U enrichment occurred was determined by EDS. In both $UMT_{6–10\ mm}$ and $UMT_{<0.45\ mm}$, U re-adsorption on aluminosilicates were observed, which were most likely albite and muscovite based on XRD results (Fig. S3). In $UMT_{6–10\ mm}$, the distribution of U was also associated with the distributions of Fe and Mg, probably with minerals like chlorite. The higher U adsorption capacity on chlorite as compared to the non-mafic assemblage in granitic rocks has been observed repeatedly (Ilton et al., 2004). An elevated amount of chlorite in $UMT_{6–10\ mm}$ might play a crucial role in U re-adsorption. Based on BSE mapping (Fig. 7c, d), elevated U content (U = 0.54%) was present in a phase (yellow color) that contained Al and Si, relative to U content (U = 0.04%) in another phase (red color) that only contained Si. This observation indicated that the affinity to aluminol during U re-adsorption was higher than that to silanol edge sites, which is in well agreement with the findings of Ilton et al. (2004) and Křepelová et al. (2007). The enrichment of U was also associated with elevated Fe contents in different phases, which might result from U(VI) reduction by Fe(II) in muscovite (Fig. 7d). Furthermore, U re-adsorption on the interlayer of mica could occur through cation exchange (Lee et al., 2009). Therefore, combined U reduction and adsorption effects of muscovite probably contributed to the elevated re-adsorbed U observed in $UMT_{<0.45\ mm}$ during the isotherm and kinetic experiments.

To reveal the underlying U re-adsorption mechanism when sulfate was added, $UMT_{6–10\ mm}$ and $UMT_{<0.45\ mm}$ samples with extensive U re-adsorption were analyzed. Their XPS U(4f) spectra were also fitted with two U(VI) and one U(IV) components (Fig. 6b and e). ~21% of total adsorbed U was U(IV) in $UMT_{<0.45\ mm}$ at pH = 8.0, while ~11% was U (IV) in $UMT_{6–10\ mm}$ at pH = 5.0. Enhanced U(VI) reduction under higher pH was also observed in Fox et al. (2013), as a result of enhanced electron transfer between Fe(II) and U(VI) at higher pH. The disappearance of muscovite in XRD spectra of both post-re-adsorption $UMT_{6–10\ mm}$ and $UMT_{<0.45\ mm}$ also suggested that muscovite was consumed during U adsorption/reduction in sulfate-containing solutions (Fig. S4). Both U-bearing phyllosilicates and mineral particles were observed in BSE images of post-re-adsorption $UMT_{6–10\ mm}$ and $UMT_{<0.45\ mm}$ in the occurrence of 0.01 M sulfate (Fig. S5). Based on XRD results, U-bearing phyllosilicates could be mainly ascribed to muscovite and chlorite (Fig. S3). The dominant roles that phyllosilicates' edge-surfaces play in U adsorption under circumneutral conditions (Sylwester et al., 2000; Hennig et al., 2002), and the elevated amounts of U re-adsorption on muscovite and chlorite relative to quartz and albite have been proved (Arnold et al., 2001). Furthermore, these two samples were oversaturated with respect to schoepite (Fig. 5b). Therefore, the U (VI) components observed in XPS could be assigned to U(VI) re-adsorption on phyllosilicates and schoepite.

The use of 0.01 M phosphate in the experiments narrowed and shifted the XPS U(4f) peaks to higher BEs as compared to the 0.01 M sulfate and 0.01 M chloride experiments. Two U(VI) components and related shake-up satellite were present in the XPS U(4f) spectra of $UMT_{6–10\ mm}$ and $UMT_{<0.45\ mm}$, whereas no U(IV) peaks were observed (Fig. 6c and f). The minor U(VI) contributor located at 382.8 eV could be ascribed to $(UO_2)_3(PO_4)_2.4\ H_2O$ precipitate (Teterin et al., 2000), which was consistent with the PHREEQC calculation (Fig. 5c). The U-containing particles observed in the BSE images of $UMT_{6–10\ mm}$ (Fig. S6a) and $UMT_{<0.45\ mm}$ (Fig. S6b) were also most likely $(UO_2)_3(PO_4)_2.4\ H_2O$ precipitate. Meanwhile, re-adsorbed U(VI) on the surface of $UMT_{6–10\ mm}$ and $UMT_{<0.45\ mm}$ observed in the BSE images probably was the main U (VI) contributor in the XPS U(4f) spectra, which accounted for ~90% of the total U.

4. Conclusions and environmental implications

Uranium containing solids including UMTs, soils, sediments and other kind of solid wastes are the primary U contamination sources in the environment. Substantial amounts of U and associated toxic metals would be mobilized from these solids due to physico-chemical weathering, posing well-known ecological risks. However, previous studies only explored the adsorption behavior of U on pure minerals (Guo et al., 2009; Singer et al., 2009; Estes and Powell, 2020; Yu et al., 2020), the re-adsorption behavior of U on actual U containing solids was rarely studied. This study showed that a considerable amount of aqueous U could be soon re-adsorbed by UMTs during leaching. The environmental hazards and ecological risks of these (waste) solids might have been underestimated resulting from the ignorance of rapid occurrence of re-adsorption, since the re-adsorbed metals would release into the environment again. Thus, the re-adsorption behavior and fundamental mechanism typical of U from UMTs under environmentally relevant conditions can provide updated understanding and more accurate assessment on the toxic U/other metals release potential and migration capacity from the solids.

The distinction in mineralogical compositions of UMTs with different particle sizes resulted in diverse interfacial conditions and mechanisms for promoting/inhibiting U re-adsorption under different conditions. The multiple mechanisms behind re-adsorption behavior illustrated in this study shed lights on U remediation strategy towards U containing (waste) solids. According to our findings, the presence of chlorite, albite and muscovite can significantly facilitate the re-adsorption process and immobilize U in the UMTs. The waste solids bearing above-mentioned minerals can enhance the capability of re-adsorbing U and other metals, and consequently mitigate the ecological risk. Moreover, our study suggests that the addition of sulfate and phosphate can also enhance the re-adsorption of leached U. These insights are helpful in developing effective in-situ remediation schemes.

CRediT authorship contribution statement

Meiling Yin: Writing - original draft, Formal analysis, Investigation. **Jing Sun**: Writing - original draft, Formal analysis. **Hongping He**: Writing - review & editing. **Juan Liu**: Writing - review & editing, Investigation. **Qiaohui Zhong**: Writing - review & editing. **Qingyi Zeng**: Writing - review & editing. **Xianfeng Huang**: Writing - review & editing. **Jin Wang**: Writing - review & editing, Supervision, Project administration. **Yingjuan Wu**: Writing - review & editing. **Diyun Chen**: Writing - review & editing.

Declaration of Competing Interest

The authors declare that they have no known competing financial interests or personal relationships that could have appeared to influence the work reported in this paper.

Acknowledgments

This study was funded by National Natural Science Foundation of China (Nos. 41773011, 41873015), Guangdong Provincial Natural Science Foundation (Nos. 2017A030313247, 2021A1515011588, 2021B1515020078), Science and Technology Planning Project of Guangdong Province, China (2020B1212060055), and the Scientific Research Projects in Colleges and Universities of Guangzhou Education Bureau, Guangzhou, China (201831803).

Appendix A. Supporting information

Supplementary data associated with this article can be found in the online version at doi:10.1016/j.jhazmat.2021.126153.

References

Abdelouas, A., 2006. Uranium mill tailings: geochemistry, mineralogy, and environmental impact. Elements 2 (6), 335–341.

ANS (American National Standard) ANSI/ANS 16.1, 1986. American National Standard for the Measurement of the Leachability of Solidified Low-level Radioactive Wastes by a Short-term Tests Procedures. American National Standards Institute, New York.

Antunes, S.C., Castro, B.B., Nunes, B., Pereira, R., Gonçalves, F., 2008. In situ bioassay with eisenia andrei to assess soil toxicity in an abandoned uranium mine. Ecotoxicol. Environ. Saf. 71 (3), 620–631.

Arnold, T., Zorn, T., Zänker, H., Bernhard, G., Nitsche, H., 2001. Sorption behavior of U (VI) on phyllite: experiments and modeling. J. Contam. Hydrol. 47 (2–4), 219–231.

Arnold, T., Utsunomiya, S., Geipel, G., Ewing, R.C., Baumann, N., Brendler, V., 2006. Adsorbed U(VI) surface species on muscovite identified by laser fluorescence spectroscopy and transmission electron microscopy. Environ. Sci. Technol. 40 (15), 4646–4652.

Ballini, M., Chautard, C., Nos, J., Phrommavanh, V., Beaucaire, C., Besancon, C., Boizard, A., Cathelineau, M., Peiffert, C., Vercouter, T., Vors, E., Descostes, M., 2020. A multi-scalar study of the long-term reactivity of uranium mill tailings from bellezane site (France). J. Environ. Radioact. 218, 106223.

Barnett, M.O., Jardine, P.M., Brooks, S.C., 2002. U(VI) adsorption to heterogeneous subsurface media: application of a surface complexation model. Environ. Sci. Technol. 36, 937–942.

Bostick, B., Fendorf, S.O., Barnett, M.M., Jardine, P., Brooks, S., 2002. Uranyl surface complexes formed on subsurface media from DOE facilities, 66 (1): 99–108.

Chang, Z., Zhou, S., 2017. Study on immobilization and migration of nuclide u in superficial soil of uranium tailings pond. In: IOP Conference Series: Earth and Environmental Science, 64. IOP Publishing, p. 12021.

Chen, B., Wang, J., Kong, L., Mai, X., Zheng, N., Zhong, Q., Liang, J., Chen, D., 2017. Adsorption of uranium from uranium mine contaminated water using Phosphate Rock Apatite (PRA): isotherm, kinetic and characterization studies. Colloids Surf. A Physicochem. Eng. Asp. 520 (2), 612–621.

Cheng, T., Barnett, M.O., Roden, E.E., Zhuang, J.L., 2004. Effects of phosphate on Uranium(VI) adsorption to goethite-coated sand. Environ. Sci. Technol. 38, 6059–6065.

Chevychelov, A.P., Sobakin, P.I., 2017. Radioactive contamination of alluvial soils in the Taiga Landscapes of Yakutia with 137Cs, 226Ra, and 238U. Eurasia Soil Sci. 50 (12), 1535–1544.

Estes, S.L., Powell, B.A., 2020. Enthalpy of uranium adsorption onto hematite. Environ. Sci. Technol. 54 (23), 15004–15012.

Fan, Q., Li, P., Chen, Y., Wu, W., 2011. Preparation and application of attapulgite/iron oxide magnetic composites for the removal of U(VI) from aqueous solution. J. Hazard. Mater. 192 (3), 1851–1859.

Fan, Q.H., Hao, L.M., Wang, C.L., Zheng, Z., Liu, C.L., Wu, W.S., 2014. The adsorption behavior of U(VI) on granite. Environ. Sci. Process. Impacts 16 (3), 534–541.

Fox, P.M., Davis, J.A., Kukkadapu, R., Singer, D.M., Bargar, J., Williams, K.H., 2013. Abiotic U (VI) reduction by sorbed Fe (II) on natural sediments. Geochim. Cosmochim. Acta 117, 266–282.

Gavrilescu, M., Pavel, L.V., Cretescu, I., 2009. Characterization and remediation of soils contaminated with uranium. J. Hazard. Mater. 163 (2–3), 475–510.

Ge, Y.B., Zhou, Z.K., Li, J.M., Li, G.C., Liu, C., Sun, Z.X., Zheng, L.L., Yang, Z.H., Rao, M. M., 2020. Combined use of $CaCl_2$ roasting and nitric acid leaching for the removal of uranium and radioactivity from uranium tailings. J. Radioanal. Nucl. Chem. 325, 657–665.

Giammar, D.E., Hering, J.G., 2001. Time scales for sorption−desorption and surface precipitation of uranyl on goethite. Environ. Sci. Technol. 35 (16), 3332–3337.

Godoy, J.M., Ferreira, P.R., Souza, E.M., de; Silva, L.I., da., Bittencourt, I., Fraifeld, F., 2019. High uranium concentrations in the groundwater of the Rio de Janeiro State, Brazil, mountainous region. J. Braz. Chem. Soc. 30 (2), 224–233.

Guenay, A., Arslankaya, E., Tosun, I., 2007. Lead removal from aqueous solution by natural and pretreated clinoptilolite: adsorption equilibrium and kinetics. J. Hazard. Mater. 146 (1–2), 362–371.

Guillaumont, R., Mompean, F.J., 2003. Update on the Chemical Thermodynamics of Uranium, Neptunium, Plutonium, Americium and Technetium. Elsevier, Amsterdam.

Guo, Z., Su, H.Y., Wu, W., 2009. Sorption and desorption of uranium (VI) on silica: experimental and modeling studies. Radiochim. Acta Int. J. Chem. Asp. Nucl. Sci. Technol. 97 (3), 133–140.

Hai, N.T., You, S.J., Hosseini-Bandegharaei, A., Chao, H.P., 2017. Mistakes and inconsistencies regarding adsorption of contaminants from aqueous solutions: a critical review. Water Res. 120, 88–116.

Hamza, M.F., 2018. Uranium recovery from concentrated chloride solution produced from direct acid leaching of calcareous shale, allouga ore materials, Southwestern Sinai, Egypt. J. Radioanal. Nucl. Chem. 315 (3), 613–626.

Hennig, C., Reich, T., Dähn, R., Scheidegger, A.M., 2002. Structure of uranium sorption complexes at montmorillonite edge sites. Radiochim. Acta 90 (9–11), 653–657.

Ho, Y.S., Mckay, G., 1999. Pseudo-second order model for sorption processes. Process Biochem. 34 (5), 451–465.

Hongxia, Z., Zuyi, T., 2002. Sorption of uranyl ions on silica: effects of contact time, pH ionic strength, concentration and phosphate. J. Radioanal. Nucl. Chem. 254 (1), 103–107.

Ilton, E.S., Haiduc, A., Moses, C.O., Heald, S.M., Elbert, D.C., Veblen, D.R., 2004. Heterogeneous reduction of uranyl by micas: crystal chemical and solution controls. Geochim. Cosmochim. Acta 68 (11), 2417–2435.

Ilton, E.S., Haiduc, A., Cahill, C.L., Felmy, A.R., 2005. Mica surfaces stabilize pentavalent uranium. Inorg. Chem. 44 (9), 2986–2988.

Ilton, E.S., Heald, S.M., Smith, S.C., Elbert, D., Liu, C., 2006. Reduction of uranyl in the interlayer region of low iron micas under anoxic and aerobic conditions. Environ. Sci. Technol. 40 (16), 5003–5009.

Jin, Q., Su, L., Montavon, G., Sun, Y., Chen, Z., Guo, Z., Wu, W., 2016. Surface complexation modeling of U(VI) adsorption on granite at ambient/elevated temperature: experimental and XPS study. Chem. Geol. 433, 81–91.

Jo, Y., Lee, J.Y., Yun, J.I., 2018. Adsorption of uranyl tricarbonate and calcium uranyl carbonate onto γ-alumina. Appl. Geochem. 94, 28–34.

Kang, M.J., Han, B.E., Hahn, P.S., 2002. Precipitation and adsorption of uranium(VI) under various aqueous conditions. Environ. Eng. Res. 7 (3), 5743–5753.

Kanzari, A., Gérard, M., Boekhout, F., Galoisy, L., Calas, G., Descostes, M., 2017. Impact of Incipient Weathering on Uranium Migration in Granitic Waste Rock Piles from Former U Mines (Limousin, France), 183, 114–126.

Kipp, G.G., Stone, J.J., Stetler, L.D., Thompson, A., Vaughan, D.J., 2009. Arsenic and uranium transport in sediments near abandoned uranium mines in Harding County, South Dakota. Appl. Geochem. 24 (12), 2246–2255.

Kong, L., Zhang, H., Shih, K., Su, M., Diao, Z., Long, J., Hou, L., Song, G., Chen, D., 2018. Synthesis of FC-supported Fe through a carbothermal process for immobilizing uranium. J. Hazard. Mater. 357, 168–174.

Korichi, S., Bensmaili, A., 2009. Sorption of uranium (VI) on homoionic sodium smectite experimental study and surface complexation modeling. J. Hazard. Mater. 169 (1), 780–793.

Křepelová, A., Brendler, V., Sachs, S., Baumann, N., Bernhard, G., 2007. U(VI)-kaolinite surface complexation in absence and presence of humic acid studied by TRLFS. Environ. Sci. Technol. 41 (17), 6142–6147.

Kuhar, LL, Bunney, K, Jackson, M, Austin, P, Li, J, Robinson, DJ, Prommer, H, Sun, J, Oram, J, Rao, A, 2018. Assessment of amenability of sandstone-hosted uranium deposit for in-situ recovery. Hydrometallurgy 179, 157–166.

Langmuir, I., 1918. The adsorption of gases on plane surfaces of glass, mica and platinum. J. Am. Chem. Soc. 40, 1361–1403.

Lee, J.-K., Baik, M.-H., Choi, J.-W., Seo, M.-S., 2011. Development of a web-based sorption database (KAERI-SDB) and application to the safety assessment of a radioactive waste disposal. Nucl. Eng. Des. 241 (12), 5316–5324.

Lee, S.Y., Baik, M.H., Lee, Y.J., Lee, Y.B., 2009. Adsorption of U(VI) ions on biotite from aqueous solutions. Appl. Clay Sci. 46 (3), 255–259.

Li, H.Y., Li, J., Ryan, J.G., Li, X., Zhao, R.P., Ma, L., Xu, Y.G., 2019b. Molybdenum and boron isotope evidence for fluid-fluxed melting of intraplate upper mantle beneath the Eastern North China Craton. Earth Planet. Sci. Lett. 520, 105–114.

Li, Z., Hadioui, M., Wilkinson, K.J., 2019a. Conditions affecting the release of thorium and uranium from the tailings of a niobium mine. Environ. Pollut. 247, 206–215.

Liang, G., Yang, Z., Shi, K., Wang, X., Guo, Z., Wu, W., 2010. U(vi) sorption on kaolinite: effects of pH u(vi) concentration and oxyanions. J. Radioanal. Nucl. Chem. 284 (3), 519–526.

Liao, R., Shi, Z.M., Chen, Y.J., Zhang, J.J., Wang, X.Y., Hou, Y., Zhang, K.L., 2020. Characteristics of uranium sorption on illite in a ternary system: effect of phosphate on adsorption. J. Radioanal. Nucl. Chem. 323, 159–168.

Liu, B., Peng, T., Sun, H., 2017. Leaching behavior of U, Mn, Sr, and Pb from different particle-size fractions of uranium mill tailings. Environ. Sci. Pollut. Res. 24 (6), 1–12.

Liu, C., Shang, J., Kerisit, S., Zachara, J.M., Zhu, W., 2013. Scale-dependent rates of uranyl surface complexation reaction in sediments. Geochim. Cosmochim. Acta 105, 326–341.

Liu, J., Wang, J., Li, H., Shen, C.C., Chen, Y., Wang, C., Ye, H., Long, J., Song, G., Wu, Y., 2015. Surface sediment contamination by uranium mining/milling activities in South China. Clean Soil Air Water 43 (3), 414–420.

Liu, J., Luo, X., Wang, J., Xiao, T., Yin, M., Belshaw, N.S., Lippold, H., Kong, L., Xiao, E., Bao, Z., 2018. Provenance of uranium in a sediment core from a natural reservoir, South China: application of Pb stable isotope analysis. Chemosphere 193, 1172–1180.

Nada, A., Imam, N., El Aassy, I.E., Ghanem, A., 2019. Effect of different concentrations of sulfuric acid on leaching of radionuclide isotopes in sedimentary rock samples, Sinai, Egypt. J. Radioanal. Nucl. Chem. 322 (2), 347–359.

Pan, D.Q., Fan, Q.H., Li, P., Liu, S.P., Wu, W.S., 2011. Sorption of Th(IV) on Na-bentonite: effects of pH ionic strength, humic substances and temperature. Chem. Eng. J. 172 (2), 898–905.

Pan, N., Tang, J., Hou, D., Lei, H., Zhou, D., Ding, J., 2021. Enhanced uranium uptake from acidic media achieved on a novel iron phosphate adsorbent. Chem. Eng. J. 423, 130267.

Payne, T.E., Davis, J.A., Waite, T.D., 1996. Uranium adsorption on ferrihydrites effects of phosphate and humic acid. Radiochim. Acta 74, 239–243.

Peng, L., Liu, P., Feng, X., Wang, Z., Cheng, T., Liang, Y., Lin, Z., Shi, Z., 2018. Kinetics of heavy metal adsorption and desorption in soil: developing a unified model based on chemical speciation. Geochim. Cosmochim. Acta 224, 282–300.

Petrescu, L., Bilal, E., 2003. Plant availability of uranium in contaminated soil from Crucea Mine (Romania). Environ. Geosci. 10 (3), 123–135.

Qiang, J., Lin, S., Montavon, G., Sun, Y., Chen, Z., Guo, Z., Wu, W., 2016. Surface complexation modeling of U(VI) adsorption on granite at ambient/elevated temperature: experimental and XPS study. Chem. Geol. 433, 81–91.

Rout, S., Ravi, P.M., Kumar, A., Tripathi, R.M., 2015. Study on speciation and salinity-induced mobility of uranium from soil. Environ. Earth Sci. 74 (3), 2273–2281.

Shao, D., Fan, Q., Li, J., Niu, Z., Wu, W., Chen, Y., Wang, X., 2009. Removal of Eu(III) from aqueous solution using ZSM-5 zeolite. Microporous Mesoporous Mater. 123 (1), 1–9.

Sharma, S.K., 2012. Health Hazards and Environmental Issues at the Uranium Mine Near Tatanagar, India BT. In: Merkel, B., Schipek, M. (Eds.), The New Uranium Mining Boom: Challenge and Lessons Learned. Springer Berlin Heidelberg, Berlin, Heidelberg, pp. 161–165.

Singer, D.M., Maher, K., Brown Jr., G.E., 2009. Uranyl–chlorite sorption/desorption: evaluation of different U(VI) sequestration processes. Geochim. Cosmochim. Acta 73 (20), 5989–6007.
Sips, R., 1948. On the structure of a catalyst surface. J. Chem. Phys. 16 (5), 490–495.
Sun, J, Bostick, BC, Mailloux, BJ, Ross, JM, Chillrud, SN, 2016. Effect of oxalic acid treatment on sediment arsenic concentrations and lability under reducing conditions. J. Hazard. Mater. 311, 125–133.
Sun, Y., Wang, D., Tsang, D.C.W., Wang, L., Ok, Y.S., Feng, Y., 2019. A critical review of risks, characteristics, and treatment strategies for potentially toxic elements in wastewater from shale gas extraction. Environ. Int. 125, 452–469.
Sylwester, E.R., Hudson, E.A., Allen, P.G., 2000. The structure of uranium (VI) sorption complexes on silica, alumina, and montmorillonite. Geochim. Cosmochim. Acta 64 (14), 2431–2438.
Teterin, Y.A., Teterin, A.Y., 2004. The structure of X-ray photoelectron spectra of light actinide compounds. Russ. Chem. Rev. 73 (6), 541–580.
Teterin, Y.A., Teterin, A.Y., Dementiev, A.P., Lebedev, A.M., Utkin, I.O., Melikhov, I.V., Nefedov, V.I., Berdonosova, D.G., Bek-Uzarov, J., Vukchevich, L., 2000. X-ray photoelectron study of the interaction of the uranyl group UO22+ with hydroxylapatite and fluoroapatite in aqueous solutions. J. Struct. Chem. 41 (4), 611–615.
Troyer, L.D., Maillot, F., Wang, Z.M., Wang, Z.M., Mehta, V.S., Giammar, D.E., Catalano, J.G., 2016. Effect of phosphate on u(vi) sorption to montmorillonite: ternary complexation and precipitation barriers. Geochim. Cosmochim. Acta 175, 86–99.
Turner, G., Zachara, J.M., Mckinley, J.P., Smith, S.C., 1996. Surface-charge properties and UO22+ adsorption of a subsurface smectite. Geochim. Cosmochim. Acta 60 (18), 3399–3414.
Wang, J., Fang, F., Zhou, Y., Yin, M., Liu, J., Wang, J., Wu, Y., Beiyuan, J., Chen, D., 2020. Facile modification of graphene oxide and its application for the aqueous uranyl ion sequestration: insights on the mechanism. Chemosphere 258, 127152.
Wang, J., Liu, J., Li, H., Song, G., Chen, Y., Xiao, T., Qi, J., Zhu, L., 2012. Surface water contamination by uranium mining/milling activities in Northern Guangdong Province, China. Clean Soil Air Water 40 (12), 1357–1363.
Wang, J., Liu, J., Li, H., Chen, Y., Xiao, T., Song, G., Chen, D., Wang, C., 2017. Uranium and thorium leachability in contaminated stream sediments from a uranium minesite. J. Geochem. Explor. 176, 85–90.
Wang, Z., Qin, H., Wang, J., 2019. Accumulation of uranium and heavy metals in the soil–plant system in Xiazhuang uranium ore field, Guangdong Province, China. Environ. Geochem. Health 41, 2413–2423.
Wang, J., Yin, M., Liu, J., Shen, C.-C., Yu, T.-L., Li, H.-C., Zhong, Q., Sheng, G., Lin, K., Jiang, X., Dong, H., Liu, S., Xiao, T., 2021. Geochemical and U-Th isotopic insights on uranium enrichment in reservoir sediments. J. Hazard. Mater. 414, 125466.
Winde, F., 2013. Uranium pollution of water: a global perspective on the situation in South Africa.
Yang, S., Zhang, X., Wu, X., Li, M., Zhang, L., Peng, Y., Huang, Q., Tan, W., 2019. Understanding the solid phase chemical fractionation of uranium in soil profile near a hydrometallurgical factory. Chemosphere 236, 124392.1–124392.10.
Yin, M., Sun, J., Wang, J., Belshaw, N., Liu, J., Linghu, W., 2019. Mechanism of uranium release from uranium mill tailings under long-term exposure to simulated acid rain: geochemical evidence and environmental implication. Environ. Pollut. 244, 174–181.
Yin, M., Tsang, D.C.W., Sun, J., Wang, J., Shang, J., Wu, Y., Liu, J., Song, G., Xiao, T., 2020. Critical insight and indication on particle size effects towards uranium release from uranium mill tailings: geochemical and mineralogical aspects. Chemosphere 250, 126315.
Yin, M., Zhou, Y., Tsang, D., Beiyuan, J., Song, L., She, J., Wang, J., Zhu, L., Fang, F., Wang, L., Liu, J., Liu, Y., Song, G., Chen, D., Xiao, T., 2021. Emergent thallium exposure from uranium mill tailings. J. Hazard. Mater. 407, 124402.
Yu, S.J., Ma, J., Shi, Y.M., Du, Z.Y., Zhao, Y.T., Tuo, X.G., Leng, Y.C., 2020. Uranium(VI) adsorption on montmorillonite colloid. J. Radioanal. Nucl. Chem. 324, 541–549.
Zhang, H., Davison, W., Knight, B., McGrath, S., 1998. In situ measurements of solution concentrations and fluxes of trace metals in soils using DGT. Environ. Sci. Technol. 32 (5), 704–710.